Stability of thermocapillary flows with inclined temperature gradient

By ALEXANDER A. NEPOMNYASHCHY[1,2],
ILYA B. SIMANOVSKII[1]† AND LEONID M. BRAVERMAN[3]

[1]Deparment of Mathematics, Technion – Israel Institute of Technology, 32000 Haifa, Israel

[2] Minerva Center for Nonlinear Physics of Complex Systems,
Technion – Israel Institute of Technology, 32000 Haifa, Israel

[3]Department of Computer Engineering, Karmiel ORT College, Karmiel, Israel

The stability of a two-layer return thermocapillary flow in the presence of an inclined temperature gradient is investigated. Both a linear stability analysis and nonlinear simulations have been performed for an air–water system. It is found that a rather weak deviation of the mean temperature gradient from the vertical direction suppresses Pearson's instability mechanism and leads to the appearance of oblique hydrothermal waves. In a certain region of parameters, transverse convective rolls drifting with the mean flow appear.

1. Introduction

The thermocapillary instability of the mechanical equilibrium in a horizontal fluid layer subject to a vertical temperature gradient (Marangoni–Bénard problem), was first investigated by Pearson (1958). Later, this problem was studied in the case of a two-layer fluid system (Smith 1966; Simanovskii & Nepomnyashchy 1993). The instability leads to the appearance of stationary convective patterns.

Another well-known problem, which was thoroughly investigated in the literature, was the instability of parallel thermocapillary flows generated by a horizontal temperature gradient. The most typical instability of such flows is connected with oblique hydrothermal waves (Smith & Davis 1983*a*; Davis 1987). These waves have been observed in experiments (Ezersky *et al.* 1993; Daviaud & Vince 1993; Garcimartín, Mukolobwiez & Daviaud 1997; Riley & Neitzel 1998), though the data concerning the propagation direction do not always coincide with the theory.

In contrast, the stability of thermocapillary flows in the presence of inclined temperature gradients has hardly been studied, unlike the case of buoyancy-induced flows (see Kelly 1994). To our knowledge, the former problem has been considered only in the limit of a large Prandtl number in the framework of the linear theory (Davis 1987), and it was investigated neither by numerical simulations nor in experiments.

In the present paper, the stability of thermocapillary flows under the joint action of vertical and horizontal temperature gradients is studied. In §2, a mathematical formulation of the problem is presented. Section 3 is devoted to the description of the linear stability results obtained for the air–water system. The numerical simulations are discussed in §4. Section 5 contains concluding remarks.

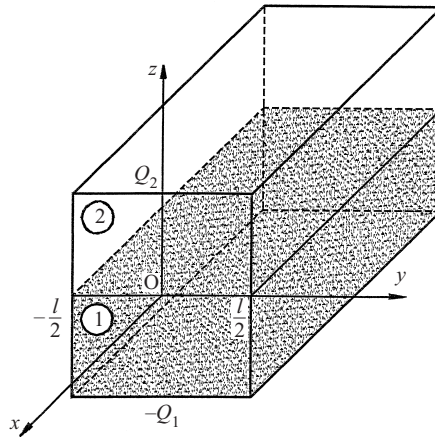† Author to whom correspondence should be addressed.

FIGURE 1. Geometrical configuration of the region and coordinate axes.
The origin O is within the front cross-section.

2. Formulation of the problem

Typically, thermocapillary flows are studied in the framework of the *one-layer* approach, i.e. the hydrodynamic and heat processes in the gas phase are neglected, and a model condition for the temperature on a free surface is used. In the present paper, a more exact *two-layer* approach is applied: all the processes are considered in both phases simultaneously.

Let the space between two parallel rigid plates at $z = -a_1$ and $z = a_2$ be filled by two immiscible viscous fluids (see figure 1). The temperature on these plates is fixed in the following way: $T(x, y, -a_1) = Ax + \Theta$, $T(x, y, a_2) = Ax$. Thus, a constant temperature gradient A is imposed in the direction of the axis x. For fixed values of x and y, the difference between the temperatures of the lower plate and the upper plate is equal to Θ. It is assumed that the interfacial tension coefficient σ decreases linearly with temperature: $\sigma = \sigma_0 - \sigma_1 T$. The buoyancy force is neglected.

The variables referring to the lower layer are marked by index 1, and those referring to the upper layer are marked by index 2. Density, kinematic and dynamic viscosity, heat conductivity, thermal diffusivity of the fluid m are, respectively, ρ_m, v_m, η_m, κ_m, and χ_m.

In the present paper the interface is assumed to be plane: $z = 0$. Strictly speaking, the interface will be perfectly flat only if horizontal pressure gradients in both fluids are equal. Generally, these gradients are not equal, so that the interface is deformed in such a way that the pressure difference generated by the thermocapillary motion is balanced by the hydrostatic pressure and the interfacial tension. However, in some cases the deformation is negligible. The relevant parameters characterizing the interface deformation are $\epsilon = Al_x\sigma_1/\sigma_0$ (Pshenichnikov & Tokmenina 1983) and $R = Al_x\sigma_1/(\rho_2 - \rho_1)ga_2$ (Tan, Bankoff & Davis 1990); g is the acceleration due to gravity, l_x is the characteristic scale of the region in the x-direction. In the present paper, we assume that these parameters are small, hence the interface deformation caused by the difference of horizontal pressure gradients can be neglected.

Under the assumption $z = 0$ we disregard the deformational instabilities discovered by Smith & Davis (1983a, b). One can expect these instabilities to be unimportant if the crispation numbers $C_j = \eta_j\chi_j/a_j\sigma_0 \ll 1$, and the Galileo numbers $G_j = ga_j^3/v_j\chi_j \gg 1$, $j = 1, 2$.

The following notation is used: $\rho = \rho_1/\rho_2$, $v = v_1/v_2$, $\eta = \eta_1/\eta_2$, $\kappa = \kappa_1/\kappa_2$, $\chi = \chi_1/\chi_2$, $a = a_2/a_1$. As the units of length, time, velocity, pressure and temperature, we use a_1, a_1^2/v_1, v_1/a_1, $\rho_1 v_1^2/a_1^2$ and Aa_1, respectively.

The complete system of nonlinear equations can be written in the following dimensionless form:

$$\left.\begin{aligned}
\frac{\partial \boldsymbol{v}_1}{\partial t} + (\boldsymbol{v}_1 \cdot \nabla)\boldsymbol{v}_1 &= -\nabla p_1 + \Delta \boldsymbol{v}_1, \\
\frac{\partial T_1}{\partial t} + \boldsymbol{v}_1 \cdot \nabla T_1 &= \frac{1}{P}\Delta T_1, \ \nabla \cdot \boldsymbol{v}_1 = 0;
\end{aligned}\right\} \tag{1}$$

$$\left.\begin{aligned}
\frac{\partial \boldsymbol{v}_2}{\partial t} + (\boldsymbol{v}_2 \cdot \nabla)\boldsymbol{v}_2 &= -\rho\nabla p_2 + \frac{1}{v}\Delta \boldsymbol{v}_2, \\
\frac{\partial T_2}{\partial t} + \boldsymbol{v}_2 \cdot \nabla T_2 &= \frac{1}{\chi P}\Delta T_2, \ \nabla \cdot \boldsymbol{v}_2 = 0,
\end{aligned}\right\} \tag{2}$$

where $P = v_1/\chi_1$ is the Prandtl number of the lower fluid.

On the rigid horizontal plates, the following boundary conditions are used:

$$z = -1: \qquad \boldsymbol{v}_1 = 0, \quad T_1 = x; \tag{3}$$

$$z = a: \qquad \boldsymbol{v}_2 = 0, \quad T_2 = x - b, \tag{4}$$

where parameter $b = \Theta/Aa_1$ describes the relation between the characteristic vertical and horizontal temperature differences. At the interface, the normal components of the velocity vanish:

$$z = 0: \quad v_{z1} = v_{z2} = 0; \tag{5}$$

and the continuity conditions for the tangential components of the velocity

$$z = 0: \quad v_{x1} = v_{x2}, \quad v_{y1} = v_{y2}, \tag{6}$$

for the tangential stresses

$$z = 0: \quad \eta\frac{\partial v_{x1}}{\partial z} = \frac{\partial v_{x2}}{\partial z} - \frac{M\eta}{P}\frac{\partial T_1}{\partial x}, \quad \eta\frac{\partial v_{y1}}{\partial z} = \frac{\partial v_{y2}}{\partial z} - \frac{M\eta}{P}\frac{\partial T_1}{\partial y}, \tag{7}$$

for the temperature

$$T_1 = T_2, \tag{8}$$

and for the heat fluxes

$$\kappa\frac{\partial T_1}{\partial z} = \frac{\partial T_2}{\partial z} \tag{9}$$

are fulfilled. Here $M = \alpha A a_1^2/\eta_1\chi_1$ is the Marangoni number.

The boundary value problem (1)–(9) has an exact solution corresponding to a parallel flow in the direction opposite to the direction of the temperature gradient:

$$\boldsymbol{v}_i = U_i^{(0)}(z)\boldsymbol{e}_x, \quad p_i = B_i^{(0)}x, \quad T_i = x + \Theta_i^{(0)}(z), \quad i = 1, 2,$$

where $\boldsymbol{e}_x$ is the unit vector on the axis x,

$$U_1^{(0)}(z) = -\frac{a\eta M\left(1 + 4z + 3z^2\right)}{4P(1 + a\eta)}, \tag{10}$$

$$U_2^{(0)}(z) = -\frac{\eta M\left(a^2 - 4az + 3z^2\right)}{4aP(1 + a\eta)}, \tag{11}$$

$$\Theta_1^{(0)}(z) = \frac{a\eta M(1+z)\left[a(a\chi+\kappa)-(1+a\kappa)\left(z+5z^2+3z^3\right)\right]}{48(1+a\eta)(1+a\kappa)} - \frac{b(z+1)}{1+a\kappa}, \quad (12)$$

$$\Theta_2^{(0)}(z) = \frac{\eta M(a-z)\left[a^2(a\chi+\kappa)+\chi(1+a\kappa)\left(a^2z-5az^2+3z^3\right)\right]}{48a(1+a\eta)(1+a\kappa)} - \frac{b(\kappa z+1)}{1+a\kappa}, \quad (13)$$

$$B_1^{(0)} = -\frac{3a\eta M}{2(1+a\eta)P}, \quad (14)$$

$$B_2^{(0)} = -\frac{3M}{2aP(1+a\eta)}. \quad (15)$$

We assume here that there are no mean longitudinal fluxes of fluids, so that

$$\int_{-1}^{0} \mathrm{d}z\, U_1^{(0)}(z) = 0, \quad \int_{0}^{a} \mathrm{d}z\, U_2^{(0)}(z) = 0. \quad (16)$$

The velocity is negative near the interface and positive near the rigid walls. On the interface, the absolute value of velocity is

$$v_s = |U_1^{(0)}(0)| = a\eta M/4P(1+a\eta). \quad (17)$$

This parallel flow is an analogue of the return thermocapillary flow considered in the one-layer approach (Davis 1987).

The temperature profiles (12) and (13) are generated by the combined action of the heat advection by the parallel flow (the terms proportional to M) and the external heating from below (the terms proportional to b). The functions $\Theta_1^{(0)}(z)$ and $\Theta_2^{(0)}(z)$ can be non-monotonic. For instance, the vertical component of the temperature gradient in the lower fluid has equal minima in the points $z = -1$ and $z = 0$:

$$\Theta_1^{(0)\prime}(-1) = \Theta_1^{(0)\prime}(0) = -\frac{a\eta M(1-\chi a^2)}{48(1+a\eta)(1+a\kappa)} - \frac{b}{1+a\kappa}, \quad (18)$$

and a maximum in the point $z = -1/3$:

$$\Theta_1^{(0)\prime}(-1/3) = \frac{a\eta M[a(a\chi+\kappa)+(7/9)(1+a\kappa)]}{48(1+a\eta)(1+a\kappa)} - \frac{b}{1+a\kappa}. \quad (19)$$

Thus, if $1 - \chi a^2 > 0$, the vertical component of the temperature gradient is negative near the boundaries $z = -1$ and $z = 0$, but it is positive in the middle of the layer, if b/M is less than a certain value. The sign of the interfacial temperature

$$\Theta_s = \Theta_1^{(0)} = \frac{\eta M a^2(a\chi+\kappa)}{48(1+a\eta)(1+a\kappa)} - \frac{b}{1+a\kappa} \quad (20)$$

is also determined by the ratio b/M. If $1 - \chi a^2 < 0$, the temperature profile is non-monotonic in the upper fluid.

The goal of the present paper is the investigation of the linear stability of the parallel thermocapillary flow (10)–(15) (§3) and the simulation of secondary flows (§4).

3. Linear stability theory

3.1. *Basic equations*

We linearize the fields of all the variables that appear in the boundary value problem (1)–(9) around the stationary solution (10)–(15):

$$\boldsymbol{v}_i(\boldsymbol{x}, z, t) = U_i^{(0)}(z)\boldsymbol{e}_x + \tilde{\boldsymbol{v}}_i(z)\exp{(\mathrm{i}\boldsymbol{k}\cdot\boldsymbol{x} + \lambda t)},$$

$$T_i(\boldsymbol{x}, z, t) = \Theta_i^{(0)}(z) + \tilde{T}_i(z)\exp{(\mathrm{i}\boldsymbol{k}\cdot\boldsymbol{x} + \lambda t)},$$

$$p_i(\boldsymbol{x}, z, t) = B_i^{(0)}x + \tilde{p}_i(z)\exp{(\mathrm{i}\boldsymbol{k}\cdot\boldsymbol{x} + \lambda t)},$$

where $\boldsymbol{x} = (x, y)$, $\boldsymbol{k} = (k_x, k_y)$ are horizontal two-dimensional vectors.

Let $k_x = k\sin\alpha$, $k_y = k\cos\alpha$. It is convenient to perform a transformation of horizontal coordinates $x = X\cos\alpha + Y\sin\alpha$, $y = -X\sin\alpha + Y\cos\alpha$. After this transformation, the wave vector $\boldsymbol{k}$ is directed along axis Y, and the disturbances do not depend on X.

We obtain the following equations for disturbances of the parallel flow:

$$\lambda\tilde{v}_{Xi} + \mathrm{i}k\sin\alpha\,U_i^{(0)}\tilde{v}_{Xi} + \cos\alpha\,U_i^{(0)\prime}\tilde{v}_{zi} = c_i(\tilde{v}_{Xi}'' - k^2\tilde{v}_{Xi}), \tag{21}$$

$$\lambda\tilde{v}_{Yi} + \mathrm{i}k\sin\alpha\,U_i^{(0)}\tilde{v}_{Yi} + \sin\alpha\,U_i^{(0)\prime}\tilde{v}_{zi} = -\mathrm{i}ke_i\tilde{p}_i + c_i(\tilde{v}_{Yi}'' - k^2\tilde{v}_{Yi}), \tag{22}$$

$$\lambda\tilde{v}_{zi} + \mathrm{i}k\sin\alpha\,U_i^{(0)}\tilde{v}_{zi} = -e_i\tilde{p}_i' + c_i(\tilde{v}_{zi}'' - k^2\tilde{v}_{zi}), \tag{23}$$

$$\lambda\tilde{T}_i + \mathrm{i}k\sin\alpha\,U_i^{(0)}\tilde{T} + \Theta_i^{(0)\prime}\tilde{v}_{zi} + \cos\alpha\,\tilde{v}_{Xi} + \sin\alpha\,\tilde{v}_{Yi} = (d_i/P)(\tilde{T}'' - k^2\tilde{T}), \tag{24}$$

$$\tilde{v}_{zi}' + \mathrm{i}k\tilde{v}_{Yi} = 0, \quad \mathrm{i} = 1, 2 \tag{25}$$

where $c_1 = d_1 = e_1 = 1$, $c_2 = 1/\nu$, $d_2 = 1/\chi$, $e_2 = \rho$, and a prime denotes differentiation with respect to z.

Introducing the stream function disturbance $\tilde{\psi}_i$, $\tilde{v}_{zi} = -\mathrm{i}k\tilde{\psi}_i$, $\tilde{v}_{Yi} = \tilde{\psi}'$ and eliminating the pressure disturbance, we obtain the following eigenvalue problem describing the stability of the parallel flow:

$$c_i(\tilde{\psi}_i'''' - 2k^2\tilde{\psi}_i'' + k^4\tilde{\psi}_i) - \mathrm{i}k\sin\alpha[U_i^{(0)}(\tilde{\psi}_i'' - k^2\tilde{\psi}_i) - U_i^{(0)\prime\prime}\tilde{\psi}_i] - \lambda(\tilde{\psi}_i'' - k^2\tilde{\psi}_i) = 0; \tag{26}$$

$$\lambda\tilde{v}_{Xi} + \mathrm{i}k\sin\alpha\,U_i^{(0)}\tilde{v}_{Xi} - \mathrm{i}k\cos\alpha\,U_i^{(0)\prime}\tilde{\psi}_i = c_i(\tilde{v}_{Xi}'' - k^2\tilde{v}_{Xi}); \tag{27}$$

$$\lambda\tilde{T}_i + \mathrm{i}k\sin\alpha\,U_i^{(0)}\tilde{T}_i - \mathrm{i}k\Theta_i^{(0)\prime}\tilde{\psi}_i + \cos\alpha\,\tilde{v}_{Xi} + \sin\alpha\,\tilde{\psi}_i' = (d_i/P)(\tilde{T}_i'' - k^2\tilde{T}_i); \tag{28}$$

$$z = -1: \quad \tilde{\psi}_1 = 0, \quad \tilde{\psi}_1' = 0, \quad \tilde{v}_{X1} = 0, \quad \tilde{T}_i = 0; \tag{29}$$

$$z = a: \quad \tilde{\psi}_2 = 0, \quad \tilde{\psi}_2' = 0, \quad \tilde{v}_{X2} = 0, \quad \tilde{T}_i = 0; \tag{30}$$

$$z = 0: \quad \tilde{v}_{X1}' - \eta^{-1}\tilde{v}_{X2}' = 0, \quad -\tilde{\psi}_1'' + \eta^{-1}\tilde{\psi}_2'' = (\mathrm{i}kM/P)\tilde{T}_1; \tag{31}$$

$$\tilde{v}_{X1} = \tilde{v}_{X2}, \quad \tilde{\psi}_1 = \tilde{\psi}_2 = 0, \quad \tilde{\psi}_1' = \tilde{\psi}_2'; \tag{32}$$

$$\tilde{T}_1 = \tilde{T}_2, \quad \kappa\tilde{T}_1' = \tilde{T}_2'. \tag{33}$$

3.2. *Discussion of results*

The calculations have been performed for a real air–water system (at $20°$ and 1 bar) with the following parameters: $\eta = 55.3$, $\nu = 0.0659$, $\kappa = 23.3$, $\chi = 0.00667$, $P = 6.96$, $a = 1$ (Perry 1997; Vargaftik 1975). In this case $1 - \chi a^2 > 0$, thus in the basic flow the vertical component of the temperature gradient in the upper layer is always negative, while in the lower layer there exists a region with a positive value
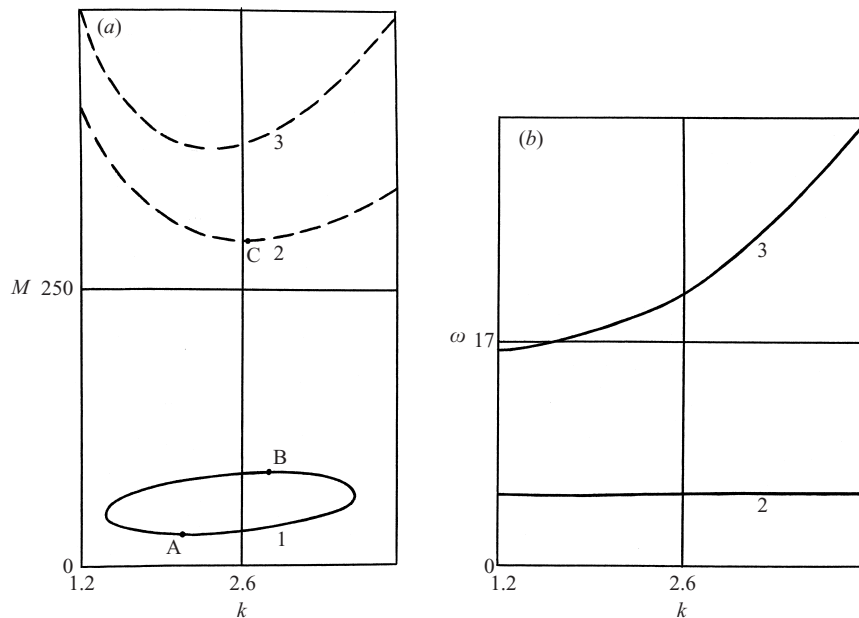
FIGURE 2. (a) Neutral curves for $b = 100$: the closed neutral curve for stationary longitudinal rolls, $\alpha = 0$ (line 1); the neutral curve for hydrothermal waves at the critical angle $\alpha = \alpha_c$ (line 2); the neutral curve for hydrothermal waves, $\alpha = 0$ (line 3). Points A and B determine the interval of existence of stationary longitudinal rolls, point C determines the onset threshold of oblique hydrothermal waves. (b) Dependence $\omega(k)$ for hydrothermal waves at $\alpha = \alpha_c$ (line 2) and at $\alpha = 0$ (line 3); $b = 100$.

of the temperature gradient, if $b/M < 0.864$. The temperature Θ_s on the interface is positive if $b/M < 0.477$ and negative in the opposite case.

In the case $b = 0$, which corresponds to the thermocapillary flow generated by a horizontal temperature gradient, the instability appears with respect to *oblique* hydrothermal waves, i.e. the direction of the critical wavevector is characterized by a certain value of α, $0 < \alpha < 90°$. These waves propagate in the direction opposite to the direction of the flow at the interface (see Smith & Davis 1983a). This type of instability is important in the interval $0 < b < b_F$, $b_F \approx 162.4$. A typical neutral curve calculated for the critical inclination angle is shown in figure 2(a) (line 2). The dependence of the frequency $\omega = \mathrm{Im}\lambda$ on the wavenumber k for the critical inclination angle is shown in figure 2(b) (line 2). The critical value of the Marangoni number M_c, which corresponds to the minimum of the neutral curve, grows from $M = M_H \approx 263.9$ when $b = 0$ to $M = M_F \approx 314.9$ when $b = b_F$ (see line 3 in figure 3), while the angle α decreases from $\alpha_H \approx 57.6°$ to $\alpha_F \approx 30°$. The critical wavenumber k_c and the critical frequency ω_c decrease slowly as b grows ($k_H \approx 2.67$, $\omega_H \approx 5.91$; $k_F \approx 2.58$, $\omega_F \approx 4.95$). Note that the phase velocity of the hydrothermal wave $v_{ph} = \omega_c/k_c$ is significantly smaller than the fluid velocity at the interface v_s (see (17)). For instance, at point H $v_{ph} \approx 2.21$, $v_s \approx 9.31$; at point F $v_{ph} \approx 1.92$, $v_s \approx 11.1$. The group velocity $v_{gr} = \mathrm{d}\omega/\mathrm{d}k$ calculated at point $k = k_c$, $M = M_c$ is rather small for hydrothermal waves (at point H $v_{gr} \approx 0.507$, at point F $v_{gr} \approx 0.0885$).

The opposite case $b \to \infty$ corresponds to Pearson's Marangoni convection (Pearson 1958) by heating from below in the absence of a horizontal component of the temperature gradient. In this limit, the critical Marangoni number $M_c \sim M'_c/b$, where M'
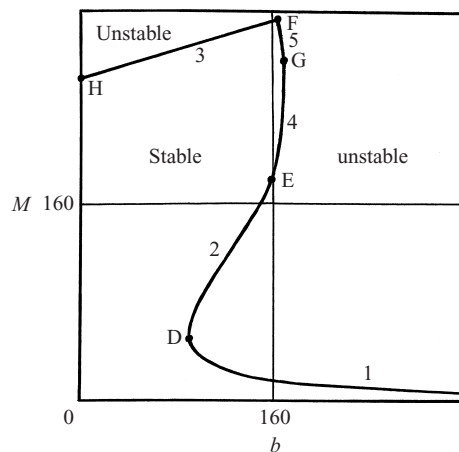
FIGURE 3. Boundaries of instability with respect to stationary longitudinal rolls ($\alpha = 0$; lines 1 and 2), oblique hydrothermal waves ($\alpha = \alpha_c$; line 3) and transverse travelling rolls ($\alpha = 90°$; lines 4 and 5). Point D corresponds to the disappearance of longitudinal rolls; point E determines the transition between longitudinal rolls and transverse travelling rolls; point F determines the transition between oblique hydrothermal waves and transverse travelling rolls; point G corresponds to the disappearance of transverse travelling rolls.

is the Marangoni number defined by means of the transverse temperature difference, which remains finite and does not depend on the direction of the wavevector. The instability is monotonic, and the stability boundary can be calculated analytically (see Smith 1966). For the air–water system with $a = 1$ $M'_c \approx 21$, $k_c \approx 2$ (see Gilev, Nepomnyashchy & Simanovskii 1987). At arbitrary large but finite b, the degeneracy of $\lambda(\alpha)$ is broken. Only longitudinal rolls with axis parallel to the horizontal component of the temperature gradient ($\alpha = 0$) grow monotonically, while any other disturbances grow in an oscillatory way because of the drift by the main flow. We have found that at large values of b the disturbances with $\alpha = 0$ are the most unstable ones. The corresponding stability boundary is shown in figure 3 (line 1).

Surprisingly, Pearson's Marangoni instability disappears at rather large values of parameter b, $b = b_D \approx 88.5$ (see point D in figure 3). Note, that for $b = b_D$ the horizontal temperature gradient is less than the *mean* vertical one by two orders of magnitude. Nevertheless, such a small horizontal temperature gradient turns out to be sufficient for complete suppression of Pearson's instability. This instability appears only at $b > b_D$ in a small closed region in the space of parameters (α, k, M) around the point $\alpha = 0$, $k = k_D \approx 2.31$, $M = M_D \approx 47.9$ (see line 1 in figure 2a). The explanation of this paradox is as follows. Because the heat conductivity of the water is much larger than that of the air ($\kappa = 23.3$), the vertical gradient in the water is actually much less than b. Using formula (20), which determines the temperature on the interface Θ_s (note that $\Theta_s \approx -b/\kappa + M/48$ since $\kappa \gg 1 \gg \chi, \eta \gg 1$) and evaluating expression (20) at point ($b = b_D$, $M = M_D$), we find that Pearson's instability is damped when the mean vertical temperature gradient *in the water layer* is only 2.7 times larger than the horizontal temperature gradient.

For the fixed value of $\alpha = 0$, the stability boundary is a closed curve in the plane (k, M) (line 1 in figure 2a), which is located much lower than the stability boundary for the hydrothermal waves (line 2 in figure 2a). The minimum and maximum points of the closed neutral curve (points A and B in figure 2a) determine the interval of

stationary instability $M_A < M < M_B$. If the heating is enhanced while maintaining constant the ratio of characteristic vertical and horizontal temperature differences b, the parallel flow first becomes unstable with respect to longitudinal rolls at $M = M_A$, but then it is *restabilized* when $M > M_B$. The parallel flow becomes unstable again (this time with respect to inclined hydrothermal waves) only for much larger values of the Marangoni number $M > M_C$, where point C corresponds to the minimum of the neutral curve for hydrothermal waves at the critical angle $\alpha = \alpha_c$ (line 2 in figure 2a). The dependence of M_A, M_B and M_C on b are presented in figure 3 (lines 1, 2 and 3, respectively). Lines 1 and 2 merge at point (b_D, M_D) (point D in figure 3).

As b increases, the interval of angles $|\alpha| < \alpha_m$ where Pearson's instability occurs, grows. At $b = b_1$, $b_1 \approx 118$, α_m reaches $90°$, i.e. at $b > b_1$ for any direction of the wavevector there exists an interval of instability. However, the critical Marangoni number M_A corresponds to $\alpha = 0$ in the whole region $b > b_D$. The maximum of the neutral surface $M = M(k, \alpha)$, M_B, corresponds to the value $\alpha = 0$ only in the interval $b_D < b < b_E$, $b_E \approx 154.6$.

For values of b slightly smaller than b_E, a new maximum appears at $\alpha = 90°$. It is caused by a new instability mode which corresponds to two-dimensional rolls directed perpendicularly to the direction of the basic flow. For $b = b_E$, both maxima have the same height $M = M_E \approx 181.5$ (see point E in figure 3). When $b > b_E$, the maximum at $\alpha = 90°$ becomes higher than the maximum at $\alpha = 0$. Thus, the lower boundary of the stability gap between the regions of Pearson's instability and the instability with respect to hydrothermal waves is connected with two-dimensional rolls. The dependence of the corresponding critical Marangoni number on b is shown in figure 3 as line 4. Similarly, when b increases, an additional minimum appears at $\alpha = 90°$ on the neutral surface $M = M(k, \alpha)$ for hydrothermal waves which competes with the minimum at $\alpha = \alpha_c$, $\alpha_c \neq 90°$. The former minimum corresponds to waves moving in the direction of the flow at the interface, i.e. to drifting rolls. Both minima provide the same critical Marangoni number $M = M_F$ when $b = b_F$ (codimension-2 point; see point F in figure 3). When $b > b_F$, the upper boundary of the stability gap is connected with two-dimensional disturbances (line 5 in figure 3) (as is its lower boundary). At $b = b_G$, $b_G \approx 164.3$, lines 4 and 5 merge with $M = M_5 \approx 276.1$ (point G in figure 3), and the stability gap disappears.

Note that for the two-dimensional instability mode described above, $\omega \neq 0$, because the rolls are driven by the basic flow. Unlike hydrothermal waves, the drifting convective rolls move in the same direction as the flow at the interface. Moreover, the phase velocity of disturbances can be even larger than the fluid velocity on the interface v_s (see (17)). At the same time, the group velocity of waves is always smaller than v_s. For instance, at point F $v_s \approx 11.1$, $v_{ph} \approx 13.4$, $v_{gr} \approx 10.1$.

Similarly, when b increases, an additional minimum appears at $\alpha = 90°$ on the neutral surface $M = M(k, \alpha)$ for hydrothermal waves which competes with the minimum at $\alpha = \alpha_c$, $\alpha_c \neq 90°$. The former minimum corresponds to waves moving in the direction of the flow at the interface, i.e. to drifting rolls. Both minima provide the same critical Marangoni number $M = M_F$ when $b = b_F$, $b_F \approx 162.4$ (codimension-2 point; see point F in figure 3). When $b > b_F$, the upper boundary of the stability gap is connected with two-dimensional disturbances (line 5 in figure 3) (as is its lower boundary).

At $b = b_G$, $b_G \approx 164.3$, lines 4 and 5 merge with $M = M_5 \approx 276.1$ (point G in figure 3), and the stability gap disappears.

The transition between the inclined hydrothermal waves moving upstream and

the two-dimensional waves moving downstream takes place at the value $b_F/M_F \approx 0.515$. Note that this value is close to the value $b/M \approx 0.477$ where the quantity Θ_s, which characterizes the mean vertical temperature gradient in water, changes its sign. Indeed, the explanation of the upstream motion of hydrothermal waves in a one-layer system (Davis 1987) is based on the fact that a downward flow generates a subsurface heating, which takes place because of the positive temperature gradient. In our case, because the heat diffusivity of air is much larger than that of water, the heat advection by a flow disturbance in air can be ignored, thus the direction of the temperature gradient in water is crucial. For relatively small b/M, the mean vertical temperature gradient in water is mainly positive, and the direction of the wave propagation can be explained as in the case of a one-layer system. For larger values of b/M, the downward flow causes a subsurface cooling, which influences the propagation direction of a temperature disturbance in the opposite way.

Let us summarize the main predictions of the linear theory. For relatively small values of b ($0 < b < b_F$) and large values of M, the excitation of inclined hydrothermal waves is expected (line 3 in figure 3). These waves move in the opposite direction to the flow at the interface. For relatively large values of b ($b > b_D$) and small values of M, the theory predicts the appearance of stationary convective rolls due to Pearson's instability (lines 1, 2 in figure 3). The axes of rolls are ordered by the thermocapillary flow along the direction of the imposed horizontal temperature gradient. For intermediate values of M, the convective rolls are ordered across the direction of the horizontal temperature gradient, and they drift with the thermocapillary flow. Unlike the hydrothermal waves, the drifting rolls move in the same direction as the flow at the interface.

4. Nonlinear simulations

4.1. *Description of the method*

We have performed numerical simulations of the flow regimes predicted by the linear stability theory.

We shall describe in more detail the numerical approach for nonlinear simulations of the longitudinal rolls (spiral flows) which appear due to the instability of the basic thermocapillary flow with respect to monotonically growing disturbances with $\alpha = 0$. One can expect that the corresponding solutions of the nonlinear boundary value problem (1)–(9) have the following structure:

$$\boldsymbol{v}_i = \boldsymbol{v}_i(y, z), \quad p_i = p_i(y, z) + B_i x, \quad T_i = x + \Theta_i(y, z), \quad i = 1, 2. \tag{34}$$

We shall assume that the motion is spatially periodic in y with a certain period $L = l/a_1$. Constants B_i are unknown and should be determined from the conditions of vanishing mean horizontal fluxes of fluids:

$$\int_{-L/2}^{L/2} \mathrm{d}y \int_{-1}^{0} \mathrm{d}z\, v_{x1}(y, z) = 0, \quad \int_{-L/2}^{L/2} \mathrm{d}y \int_{0}^{a} \mathrm{d}z v_{x2}(y, z) = 0. \tag{35}$$

For spiral flows (34) the continuity equations

$$\frac{\partial v_{yi}}{\partial y} + \frac{\partial v_{zi}}{\partial z} = 0, \quad i = 1, 2,$$

do not include v_{xi}. That is why it is possible to define the stream functions ψ_i of the

transverse flow in the following way:

$$v_{yi} = \frac{\partial \psi_i}{\partial z}, \quad v_{zi} = -\frac{\partial \psi_i}{\partial y}. \tag{36}$$

After elimination of the pressure fields $p_i(y, z)$ in the usual manner, we obtain the following nonlinear boundary value problem:

$$\frac{\partial}{\partial t} \Delta_\perp \psi_i + \frac{\partial \psi_i}{\partial z} \frac{\partial}{\partial y} \Delta_\perp \psi_i - \frac{\partial \psi_i}{\partial y} \frac{\partial}{\partial z} \Delta_\perp \psi_i = c_i \Delta_\perp^2 \psi_i; \tag{37}$$

$$\frac{\partial}{\partial t} U_i + \frac{\partial \psi_i}{\partial z} \frac{\partial}{\partial y} U_i - \frac{\partial \psi_i}{\partial y} \frac{\partial}{\partial z} U_i = c_i \Delta_\perp^2 U_i - e_i B_i; \tag{38}$$

$$\frac{\partial}{\partial t} \Theta_i + \frac{\partial \psi_i}{\partial z} \frac{\partial}{\partial y} \Theta_i - \frac{\partial \psi_i}{\partial y} \frac{\partial}{\partial z} \Theta_i + U_i = \frac{d_i}{P} \Delta_\perp \Theta_i; \tag{39}$$

$$z = -1: \quad \psi_1 = 0, \quad \frac{\partial \psi_1}{\partial z} = 0, \quad U_1 = 0, \quad \Theta_1 = 0; \tag{40}$$

$$z = a: \quad \psi_2 = 0, \quad \frac{\partial \psi_2}{\partial z} = 0, \quad U_2 = 0, \quad \Theta_2 = -b; \tag{41}$$

$$z = 0: \quad \psi_1 = \psi_2 = 0, \quad \frac{\partial \psi_1}{\partial z} = \frac{\partial \psi_2}{\partial z}, \quad U_1 = U_2; \tag{42}$$

$$\eta \frac{\partial^2 \psi_1}{\partial z^2} = \frac{\partial^2 \psi_2}{\partial z^2} - \frac{M\eta}{P} \frac{\partial \Theta_1}{\partial y}; \tag{43}$$

$$\eta \frac{\partial U_1}{\partial z} = \frac{\partial U_2}{\partial z} - \frac{M\eta}{P}; \tag{44}$$

$$\Theta_1 = \Theta_2; \tag{45}$$

$$\kappa \frac{\partial \Theta_1}{\partial z} = \frac{\partial \Theta_2}{\partial z}; \tag{46}$$

$$\psi_i(y + L, z) = \psi_i(y, z), \quad U_i(y + L, z) = U_i(y, z), \quad \Theta_i(y + L, z) = \Theta_i(y, z), \quad i = 1, 2, \tag{47}$$

where

$$\Delta_\perp = \frac{\partial^2}{\partial y^2} + \frac{\partial^2}{\partial z^2}, \quad U_i = v_{xi}, \quad c_1 = d_1 = e_1 = 1, \quad c_2 = 1/\nu, \quad d_2 = 1/\chi, \quad e_2 = \rho.$$

Constants B_i ($i = 1, 2$) should be found from the conditions

$$\int_{-L/2}^{L/2} dy \int_{-1}^{0} dz\, U_1 = 0, \quad \int_{-L/2}^{L/2} dy \int_{0}^{a} dz\, U_2 = 0. \tag{48}$$

For the calculation of B_i and the fields U_i that satisfy conditions (48), the following procedure is applied. Functions U_i are presented in the form

$$U_i = \tilde{U}_i + \sum_{j=1}^{2} e_j B_j V_{ij}, \quad i = 1, 2, \quad j = 1, 2, \tag{49}$$

where $\tilde{U}_i$ and V_{ij} satisfy the following equations and boundary conditions:

$$\frac{\partial}{\partial t}\tilde{U}_i + \frac{\partial \psi_i}{\partial z}\frac{\partial}{\partial y}\tilde{U}_i - \frac{\partial \psi_i}{\partial y}\frac{\partial}{\partial z}\tilde{U}_i = c_i\Delta_\perp U_i; \tag{50}$$

$$z = -1: \quad \tilde{U}_1 = 0: \quad z = a: \quad \tilde{U}_2 = 0; \tag{51}$$

$$z = 0: \quad \tilde{U}_1 = \tilde{U}_2, \quad \eta\frac{\partial \tilde{U}_1}{\partial z} = \frac{\partial \tilde{U}_2}{\partial z} - \frac{M\eta}{P}; \tag{52}$$

$$\tilde{U}_i(y + L, z) = \tilde{U}_i(y, z), \tag{53}$$

$$\frac{\partial}{\partial t}V_{ij} + \frac{\partial \psi_i}{\partial z}\frac{\partial}{\partial y}V_{ij} - \frac{\partial \psi_i}{\partial y}\frac{\partial}{\partial z}V_{ij} = c_i\Delta_\perp V_{ij} - \delta_{ij} - \frac{\partial \ln B_j}{\partial t}V_{ij}; \tag{54}$$

$$z = -1: \quad V_{1j} = 0: \quad z = a: \quad V_{2j} = 0; \tag{55}$$

$$z = 0: \quad V_{1j} = V_{2j}, \quad \eta\frac{\partial V_{1j}}{\partial z} = \frac{\partial V_{2j}}{\partial z}; \tag{56}$$

$$V_{ij}(y + L, z) = V_{ij}(y, z), \tag{57}$$

$i = 1, 2$; $j = 1, 2$; and δ_{ij} is the Kronecker symbol. After the calculation of $\tilde{U}_i$ and V_{ij} (the last term in (54) is evaluated from the previous time steps), expression (49) is substituted into conditions (48), and the system of two linear algebraic equations for B_j is solved.

Solutions of the boundary value problem (37)–(48) are obtained by the finite difference method. The 'stream function–vorticity' variables are used to solve equation (37) with corresponding boundary conditions (for details, see Simanovskii & Nepomnyashchy 1993). Equations and boundary conditions (37)–(47) are approximated on a uniform mesh using a second-order approximation for the spatial coordinates. The integration of evolution equations is performed by means of an explicit scheme. The rectangular mesh 28×56 was used. The time step was chosen from the stability conditions.

For simulation of inclined hydrothermal waves, we performed the transformation of variables

$$x = X\cos\alpha + Y\sin\alpha, \quad y = -X\sin\alpha + Y\cos\alpha \tag{58}$$

and presented the solution in the form

$$\boldsymbol{v}_i = \boldsymbol{v}_i(Y, z), \quad p_i = p_i(Y, z) + B_iX, \quad T_i = X\cos\alpha + Y\sin\alpha + \Theta_i(Y, z), \quad i = 1, 2. \tag{59}$$

In this case, equation (39) is replaced by the following equation:

$$\frac{\partial}{\partial t}\Theta_i + \frac{\partial \psi_i}{\partial z}\left(\frac{\partial}{\partial y}\Theta_i + \sin\alpha\right) - \frac{\partial \psi_i}{\partial y}\frac{\partial}{\partial z}\Theta_i + U_i\cos\alpha = \frac{d_i}{P}\Delta_\perp\Theta_i, \tag{60}$$

and boundary conditions (43), (44) take the form

$$\eta\frac{\partial^2\psi_1}{\partial z^2} = \frac{\partial^2\psi_2}{\partial z^2} - \frac{M\eta}{P}\left(\frac{\partial}{\partial y}\Theta_1 + \sin\alpha\right), \tag{61}$$

$$\eta\frac{\partial U_1}{\partial z} = \frac{\partial U_2}{\partial z} - \frac{M\eta}{P}\cos\alpha. \tag{62}$$

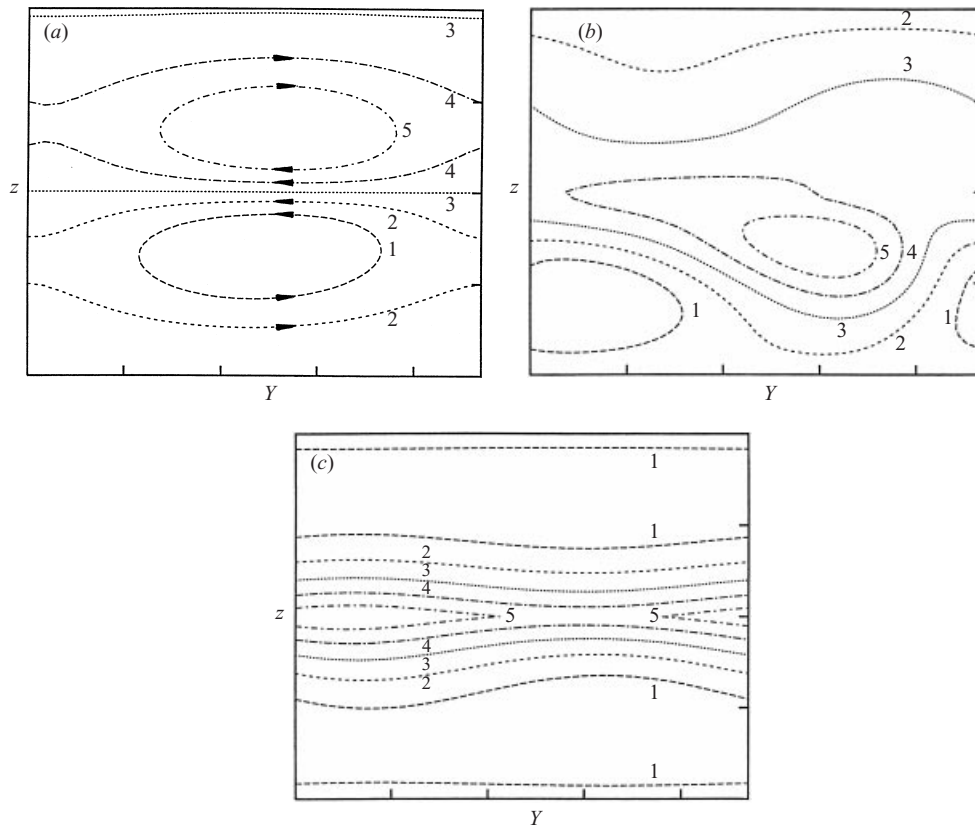The boundary value problem obtained was solved in the same way as in the case of longitudinal rolls.

FIGURE 4. Isolines for inclined hydrothermal waves. (*a*) The stream function: 0.0706 (1), 0.035 (2), -0.0006 (3), -0.0362 (4), -0.0717 (5); (*b*) the temperature disturbance: 0.00294 (1), -0.00188 (2), -0.0067 (3), -0.0115 (4), -0.0163 (5); (*c*) the longitudinal velocity: 0.0796 (1), -0.0688 (2), -0.217 (3), -0.366 (4), -0.514 (5). $M = 328$, $b = 100$, $\alpha = 41°$, $L = 2.35$.

In the simulation of drifting transverse rolls α was taken equal to $90°$ in equations (58)–(62).

4.2. *Numerical results*

We have investigated the nonlinear flow regimes for the same fluid system as in § 3.2.

First, let us consider the hydrothermal waves with an oblique wavevector ($0 < \alpha < 90°$). This type of wave is developed for relatively small values of b/M, when there exists a region with a positive vertical component of the temperature gradient in the lower layer, and the interfacial temperature Θ_s is positive (see (20)). Snapshots of the fields of the stream functions $\psi_i(Y, z)$, the *disturbances* of the temperature $\Theta_i(Y, z) - \Theta_i^{(0)}(z)$, and the longitudinal velocity $U_i(Y, z)$ ($i = 1, 2$) are shown in figure 4. For technical reasons, the non-dimensional values of ψ_i, U_i and $\Theta_i - \Theta_i^{(0)}$ are given in units v_2, v_2/a_2 and Θ, respectively. The motion is a travelling wave, $f_i(Y, z, t) = f_i(Y - ct, z)$, $i = 1, 2$, where $f_i = (\psi_i, U_i, \Theta_i - \Theta_i^{(0)})$, with a positive phase velocity c, i.e. the waves move in the direction opposite to the Y-component of the flow velocity at the interface. The explanation of this phenomenon given by Davis (1987) is based on the fact that the vertical component of the temperature gradient in water is positive in a certain region. Let us consider the fields of
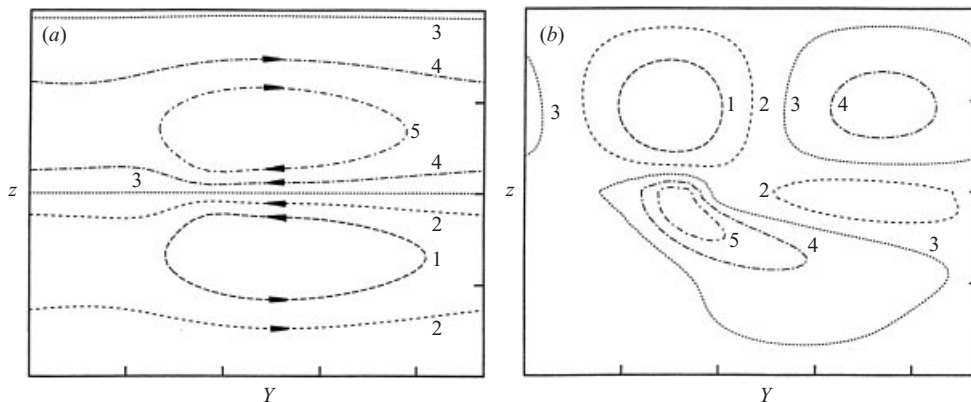
FIGURE 5. Isolines for transverse travelling rolls (*a*) The stream function: 0.0619 (1), 0.0306 (2), −0.0007 (3), −0.0319 (4), −0.0632 (5); (*b*) the temperature disturbance: 0.00138 (1), 0.00051 (2), −0.00036 (3), −0.00123 (4), −0.0021 (5). $M = 200$, $b = 200$, $\alpha = 90°$, $L = 2.35$.

variables shown in figures 4(*a*) and 4(*b*). A negative disturbance of the *interfacial* temperature is situated to the left of the computation region centre (see figure 4*b*), and it generates a corresponding descending motion in the water. Because of the incompressibility of the fluid, an ascending motion appears in the region to the right of the centre (see figure 4*a*). The latter flow leads to a cooling in the region under the interface, where the vertical component of the temperature gradient is positive. This effect tends to shift the minimum of the interfacial temperature to the right. That is why the wave moves to the right, despite the advection of the interfacial temperature field by the Y-component of the interfacial velocity. Because of the large thermal diffusivity of air, the influence of the motion in the upper fluid can be neglected.

Let us discuss now the results of nonlinear simulations of two-dimensional (transverse) rolls moving in the same direction as the interfacial flow. This kind of wave appears at larger values of b/M, where the region of a positive vertical temperature gradient is relatively small, and the sign of the interfacial temperature (20) in water is negative (i.e. the external heating from below dominates the heating from above caused by the basic flow). The snapshots of the fields of variables are shown in figure 5. Let us emphasize that the temperature in the region of an ascending flow is now higher than that in the region of a descending flow. Thus, the mechanism driving the wave in the direction opposite to the interfacial flow is switched off. The minimum of the interfacial temperature now moves in the same direction as the interfacial flow, i.e. the wave moves to the left ($c < 0$).

Finally, let us consider longitudinal rolls (spiral flows). The simulations have been done for $b = 100$ and $L = 2.75$ (i.e. $k = 2\pi/L \approx 2.285$). The linear theory predicts an instability in the interval between $M = M_A \approx 28.47$ (with the critical wavenumber $k = 2.11$) and $M = M_B \approx 82.59$ (with the critical wavenumber $k = 2.825$). The numerical simulations reveal the existence of stable spiral flows with the chosen period L in the interval $M_1 < M < M_2$, $M_1 \approx 30$, $M_2 \approx 80$. No subcritical flows have been found, neither when $M > M_A$ nor when $M < M_B$. Thus, the prediction of the linear theory concerning the restabilization of the parallel flow above the line 2 of figure 3 has been verified by our numerical simulations. The isolines of the stream function fields ψ_i and the longitudinal velocity fields U_i calculated for $M = 61.2$ are

----- 0.00438
------- 0.00219
------- 3.14×10^{-8}
----- −0.00219
----- −0.00438

----- 0.0174
------- −0.0184
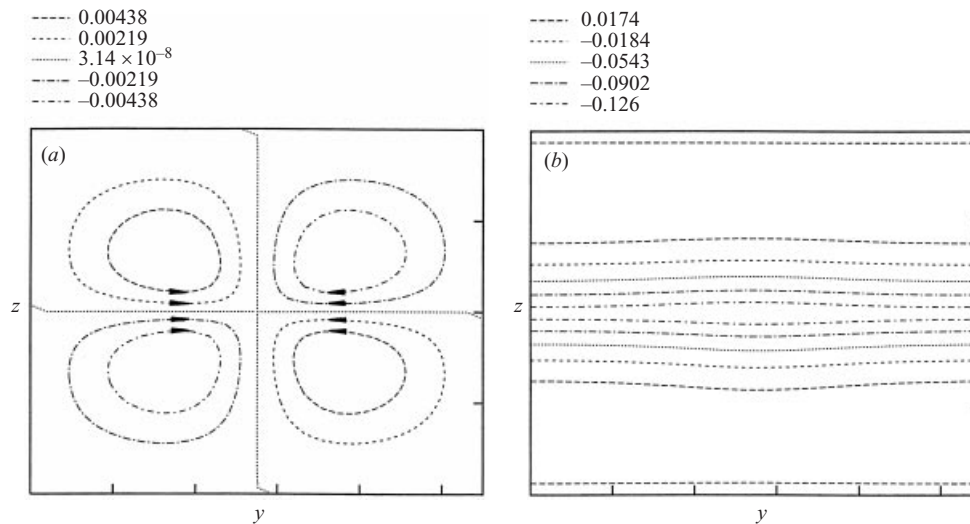------- −0.0543
----- −0.0902
----- −0.126

FIGURE 6. Isolines of (*a*) the stream function fields and (*b*) longitudinal velocity fields for periodic stationary spiral flow at $M = 61.2$, $b = 100$, $\alpha = 0$, $L = 2.75$.

shown in figure 6. The secondary motion $\psi_i(y, z)$ has a four-vortex structure. The fields of variables satisfy the following symmetry conditions:

$$\psi_i(y, z) = -\psi_i(-y, z), \quad U_i(y, z) = U_i(-y, z), \quad \Theta_i(y, z) = \Theta_i(-y, z). \tag{63}$$

5. Conclusions

The stability of the return thermocapillary flow in an air–water system with an imposed inclined temperature gradient has been investigated. Three instability modes have been found: oblique hydrothermal waves, longitudinal rolls and two-dimensional waves. We predict several effects that could be observed in experiments.

Because of the large difference between heat conductivities of air and water, a very small (about 1%) horizontal component of the mean temperature gradient is sufficient for a full suppression of Pearson's instability in the form of longitudinal rolls.

In a certain region of parameter b (this parameter characterizes the ratio between the longitudinal and vertical components of the temperature gradient) the neutral curve for Pearson's instability is closed. Thus, the longitudinal rolls exist in a bounded interval of Marangoni numbers, i.e. the parallel flow is *restabilized* with the growth of the temperature gradient.

In addition to oblique hydrothermal waves and longitudinal rolls, we predict the appearance of transverse rolls drifting with the flow, in a certain region of parameters.

Preliminary experiments on the convective flows in a liquid layer with an inclined temperature gradient have been done recently by A. B. Ezersky (2000, personal communication). A transition between longitudinal rolls and waves moving in the direction of the interfacial flow has been observed. The verification of theoretical predictions given in the present paper needs additional experiments.

REFERENCES

DAVIAUD, F. & VINCE, J. M. 1993 Traveling waves in a fluid layer subjected to a horizontal temperature gradient. *Phys. Rev.* E **48**, 4432.

DAVIS, S. H. 1987 Thermocapillary instabilities. *Ann. Rev. Fluid Mech.* **19**, 403.

EZERSKY, A. B., GARCIMARTÍN, A., MANCINI, H. L. & PÉREZ-GARCÍA, C. 1993 Spatiotemporal structure of hydrothermal waves in Marangoni convection. *Phys. Rev.* E **48**, 4414.

GARCIMARTÍN, A., MUKOLOBWIEZ, N. & DAVIAUD, F. 1997 Origin of waves in surface-tension-driven convection. *Phys. Rev.* E **56**, 1699.

GILEV, A. YU., NEPOMNYASHCHY, A. A. & SIMANOVSKII, I. B. 1987 Generation of thermocapillary and thermogravitational convection in an air-water system. *Fluid Mech.-Sov. Res.* **16**, 44.

KELLY, R. E. 1994 The onset and development of thermal convection in fully developed shear flows. *Adv. Appl. Mech.* **31**, 35.

PEARSON, J. R. A. 1958 On convection cells induced by surface tension. *J. Fluid Mech.* **4**, 489.

PERRY, R. H. 1997 *Perry's Chemical Engineers' Handbook*. McGraw-Hill.

PSHENICHNIKOV, A. F. & TOKMENINA, G. A. 1983 Deformation of the free surface of a liquid by thermocapillary motion. *Fluid Dyn.* **18**, 463.

RILEY, R. J. & NEITZEL, G. P. 1998 Instability of thermocapillary-buoyancy convection in shallow layers. Part 1. Characterization of steady and oscillatory instabilities. *J. Fluid Mech.* **359**, 143.

SIMANOVSKII, I. B. & NEPOMNYASHCHY, A. A. 1993 *Convective Instabilities in Systems with Interface*. Gordon and Breach.

SMITH, K. A. 1966 On convective instability induced by surface-tension gradients. *J. Fluid Mech.* **24**, 401.

SMITH, M. K. & DAVIS, S. H. 1983a Instabilities of dynamic thermocapillary liquid layers. Part 1. Convective instabilities. *J. Fluid Mech.* **132**, 119.

SMITH, M. K. & DAVIS, S. H. 1983b Instabilities of dynamic thermocapillary liquid layers. Part 2. Surface-wave instabilities. *J. Fluid Mech.* **132**, 145.

TAN, M. J., BANKOFF, S. G. & DAVIS, S. H. 1990 Steady thermocapillary flows of thin liquid layers, *Phys. Fluids* A **2**, 313.

VARGAFTIK, N. B. 1975 *Tables on the Thermophysical Properties of Liquids and Gases*. Hemisphere.